Contents lists available at ScienceDirect

Ceramics International

journal homepage: www.elsevier.com/locate/ceramint

Moderate temperature sintering of $BaZr_{0.8}Y_{0.2}O_{3-\delta}$ protonic ceramics by A novel cold sintering pretreatment

Zeyu Zhao, Jun Gao, Yuqing Meng, Kyle S. Brinkman, Jianhua Tong [*]

Department of Materials Science and Engineering, Clemson University, Clemson, SC, 29634, USA

ARTICLE INFO

ABSTRACT

The state-of-the-art protonic ceramic conductor $BaZr_{0.8}Y_{0.2}O_{3-\delta}$ (BZY20) requires an extremely high sintering temperature (≥ 1700 °C) to achieve the desired relative density and microstructure necessary to function as a proton conducting electrolyte. In this work, we developed a cold sintering pretreatment assisted moderate-temperature sintering method for the fabrication of high-quality pure BZY20 pellets. BZY20 pellets with high relative density of ~94% were fabricated with a final sintering temperature of 1500 °C (200 °C lower than the traditional sintering temperature). A comparison with BZY20 control samples indicated that the proper amount of $BaCO_3$ introduced on the BZY20 particle surface and the high green density achieved by cold sintering pretreatment were the main drivers for lowering the sintering temperature. The electrical conductivity measurement by electrochemical impedance spectroscopy showed that the as-prepared BZY20 pellets have a proton conductivity comparable to the state-of-the-art values. The cold sintering pretreatment outlined in this work has the potential to lower the sintering temperatures for similar types of protonic ceramic materials under consideration for a wide range of energy conversion and storage applications.

1. Introduction

Proton conducting oxides (i.e., protonic ceramics, PCs) have attracted increasing attention in energy conversion and storage devices [1–4] due to their high ionic conductivity at intermediate temperatures (300–600 °C) as compared with traditional oxygen-ion conducting materials [5]. Among the versatile PC materials, the perovskite oxides of doped barium cerates and zirconates, such as $BaCe_{0.8}Y_{0.2}O_{3-\delta}$ (BCY20), $BaCe_{0.8}Gd_{0.2}O_{3-\delta}$ (BCG20), $BaCe_{1-x-y}Zr_xY_yO_{3-\delta}$ (BCZY), $BaCe_{0.7}Zr_{0.1}Y_{0.1}Yb_{0.1}O_{3-\delta}$ (BCZYYb7111), $BaCe_{0.4}Zr_{0.4}Y_{0.1}Yb_{0.1}O_{3-\delta}$ (BCZYYb4411), $BaCe_{0.7}Zr_{0.1}Y_{0.07}Sm_{0.13}O_{3-\delta}$ (BCZYSm), and $BaZr_{1-x}Y_xO_{3-\delta}$ (BZY), represent state-of-the-art materials [6]. The majority of doped barium cerates (e.g., BCY20 and BCG20) usually exhibit high proton conductivity, however, these materials often suffer from poor chemical stability when exposed to water and carbon dioxide containing atmospheres [7]. The introduction of the proper amount of zirconium into doped barium cerates improved the chemical stability to some degree while maintaining appreciable levels of proton conductivity (e.g., BCZY and BCZYYb) [8]. However, fuel cell operation with hydrocarbon fuels (e.g., methane) rapidly degraded the BCZYYb7111 based materials [9], and some fuel cells based on BCZY with different Ce/Zr radios exhibited problems with stability and long term operation [10].

In contrast, the yttrium doped barium zirconates BZY show excellent chemical stability as compared with doped barium cerates and their derivatives. The study on single-crystal samples and epitaxial thin films of BZY demonstrated excellent proton conductivity, which was even higher than the values obtained for doped barium cerates [11]. However, their refractory nature demanded a high sintering temperatures around 1700 °C to obtain an acceptable relative density in order to function as the electrolyte [12]. The high sintering temperature resulted in significant barium loss from the bulk and Y_2O_3 precipitation in the grain boundaries, which inevitably caused low proton conductivity for the BZY electrolytes [13]. Many efforts have been pursued over the decades to achieve BZY samples with high relative density and the desired microstructure. Processing under flowing pure oxygen with a protection powder bath (90 wt% BYZ20 and 10 wt % $BaCO_3$) was a novel and promising method to prepare dense BZY pellets from powders synthesized via wet-chemistry, which require a sintering temperature around 1600 °C to achieve the acceptable relative density [14]. Spark plasma sintering was a powerful tool to achieve high relative density while limiting the grain size growth. The spark plasma sintering method

usually resulted in high relative densities for BZY pellets, which showed a comparable proton conductivity to the samples obtained from the conventional sintering method [15,16]. However, spark plasma sintering requires complex equipment, high cost, and faces limitations with sample geometries, making it challenging to utilize for the fabrication of protonic ceramic devices. The pulsed laser deposition technique showed the capability to achieve epitaxial dense BZY thin film exhibiting high proton conductivity [17]. Nonetheless, this technique needs to address similar challenges as spark plasma sintering before its practical application. In recent years, the solid state reactive sintering based on sintering aids such as NiO [18], ZnO [12], CoO [19], and CuO [20] significantly lowered the sintering temperatures of PCs, including BZY. The sintering temperatures lower than or equal to 1500 °C ensured the successful fabrication of PC devices, which showed promising device performance. Specifically, BZY-based devices fabricated by the solid state reactive sintering method showed both excellent chemical stability and power density. However, the addition of sintering aids resulted in mechanical instability and made it difficult to study the intrinsic properties of BZY [21]. Therefore, the PC community still needs a new sintering method to achieve dense, phase pure BZY samples at moderate sintering temperatures ($\leq$1500 °C).

A new technique, named cold sintering, was developed to obtain dense ceramics at temperatures much lower than the traditional sintering temperatures to densify ceramics at extraordinarily low temperatures of $\leq$300 °C. The cold sintering process utilizes a small amount of water vapor or aqueous environments as a transient solvent. The addition of water improved the rearrangement of particles and boosted mass transfer [22]. Cold sintering showed promising sintering results for a broad series of ceramics such as ZnO, Li_2CO_3, $LiFePO_4$, $BaTiO_3$, and $Li_{0.5x}Bi_{1-0.5x}Mo_xV_{1-x}O_4$. For example, dense ZnO pellets were prepared by cold sintering at a temperature lower than 300 °C, which is 700 °C lower than the traditional sintering temperature of ~1000 °C [23]. The cold sintering pretreatment of $BaTiO_3$ at a temperature around 180 °C could help densify $BaTiO_3$ after post-sintering at 900 °C, which was 500 °C lower than the traditional sintering temperature (~1400 °C) [24]. The formation of an amorphous $BaTiO_3$ layer on particle surface from the coated $Ba(OH)_2$ and TiO_2 aqueous suspension during the cold sintering was proposed to be the reason why post-sintering at 900 °C could fully densify $BaTiO_3$. In the most recent work, a conventional PC material of $BaCe_{0.9}Zr_{0.1}Y_{0.1}O_{3-\delta}$ was fully densified by combining the cold sintering treatment at 200 °C followed by sintering at 1200 °C, which was 300 °C lower than the traditional sintering temperature of 1500 °C [25]. However, until now, the cold sintering technique has not been successfully utilized to densify BZY protonic ceramic at moderate temperatures ($\leq$1500 °C).

In this work, we applied the cold sintering pretreatment process on as-synthesized phase-pure BZY20 powder by the modified Pechini method to achieve BZY20 pellets with a relative density of ~94%. The cold sintering pretreatment was carried out in the 20 wt% of water environment at a temperature of 180 °C under ~400 MPa pressure, and the subsequent sintering was at a temperature of 1500 °C in a box furnace. The conductivity measurement and analysis showed that the as-prepared dense BZY20 pellets have comparable proton conductivities with the state-of-the-art BZY20 pellets. A mechanism of the cold sintering induced reduction in the final densification temperature while preserving the desired microstructure is proposed. We expect that the same methodology for preparing dense BZY20 will result in similar densification results for other perovskite-type protonic ceramics.

2. Experimental

2.1. Synthesis of BZY20 powder

$BaZr_{0.8}Y_{0.2}O_{3-\delta}$ (BZY20) powder was synthesized by the modified Pechini method described in our previous work [1]. Stoichiometric amounts of $Ba(NO_3)_2$ (99+% Alfa Aesar), $ZrO(NO_3)_2$ solution (~35 wt

%, Sigma Aldrich), and $Y(NO_3)_3$ (99.9%, Alfa Aesar) were mixed into the proper amount of deionized water in a beaker. Ethylenediaminetetra-acetic acid (EDTA, 99.4%, Alfa Aesar) and citric acid monohydrate (99.5%, ACROS Organics) were added to the nitrate solution with magnetic stirring. The molar ratios of EDTA and citric acid to the total cation are both 1.5 and 1, respectively. The solids dissolved and formed a clear solution after slowly adding ammonium hydroxide ($NH_3 \cdot H_2O$, 28–30% w/w, LabChem) to adjust pH around 10. With gradual water vaporization at 80–90 °C on a hot plate, the solution finally turned into a viscous gel. After further drying at 150 °C for 48 h in a box oven, the gel turned into a dark charcoal-like primary powder, which eventually calcined at 900 °C for 10 h to form crystalized BZY20 perovskite precursor powder.

2.2. Preparation of BZY20 pellets

The as-synthesized BZY20 powder was mixed with a certain amount of polyvinyl alcohol (PVA, Alfa Aesar) aqueous solution (3 wt% PVA in deionized water) to achieve the water amount as 20 wt% of the total powder weight. Around 0.8 g of this wet BZY20 powder was evenly packed in circular carbon-aided steel die set with a diameter of 12.7 mm. The pressing was firstly performed under ~400 MPa at room temperature for 10 min. The die set was then heated to 180 °C with a ramp rate of 10 °C/min by a heating tape and held for 1 h to perform the cold sintering pretreatment under the same pressure. The cold-sintered pellets were placed in the box furnace overnight at 200 °C to remove residual absorbed water. The subsequent sintering was performed at a moderate temperature of 1500 °C for 12 h to achieve final BZY20 pellets marked as CS-20. Simultaneously, three control BZY20 pellets were also prepared from the as-synthesized BZY20 powder for comparison. One control BZY20 pellet named CS-0 was fabricated via the same procedure for CS-20 except that no water was added to the powder. The other two control BZY20 pellets were prepared under traditional sintering conditions. The as-prepared BZY20 powder with 20 wt% water or without water addition was pressed under ~400 MPa for 10 min in circular carbon-aided steel die set with a diameter of 12.7 mm to form green pellets, which were further sintered at 1500 °C for 12 h to achieve sintered BZY20 pellets. These two BZY20 pellets were named TS-0 and TS-20. For convenience, experimental conditions for each investigated pellet were summarized in Table 1.

2.3. Characterization

A Rigaku Ultima IV diffractometer, using monochromatic Cu Kα radiation (1.5406 Å), was employed to record the X-ray diffraction (XRD) patterns for all BZY20 pellet samples. The scanning rate was 1°/min with a step length of 0.02° and a 2θ scan range of 20°~80°. The microstructures of BZY20 samples were observed by scanning electron microscopy (SEM) of a Hitachi S-4800 microscope under 10 kV acceleration voltage and emission current of 10 μA. Element compositions inside all samples were detected by the Energy Dispersive X-Ray Spectroscopy (EDX) (Oxford) component on S-4800 with 20 kV acceleration voltage and emission current of 15 μA.

Table 1
The summary of experimental conditions for BZY20 pellets.

Sample	H$_2$O amount (wt%)	Pretreatment Condition	Sintering Condition
CS-0	0	400 MPa 10 min at RT and 1 h at 180 °C	1500 °C 12 h
CS-20	20		
TS-0	0	400 MPa 10 min at RT	
TS-20	20		

2.4. Electrochemical measurement

Symmetrical cells for conductivity test were fabricated in the electrode | electrolyte | electrode configuration. The silver paste (Alfa Aesar, item number 44075) was applied on both sides of a BZY20 pellet by a screen printing method. Silver mesh (Alfa Aesar, item number 40936) and gold wire (Alfa Aesar, item number 00725) were attached to the sliver electrode surfaces to work as current collectors and lead wires (four probes), respectively. The pellet was dried on a hot plate at 150 °C for good adherence. The electrochemical impedance spectra (EIS) for BZY20 pellets were measured by a Gamry Reference 600 Plus at 300ᵒC–700 °C under several atmospheres, including wet air, wet 5% H_2 (balanced by Ar), dry air, and dry 5% H_2 with a flow rate of 50 mL min^{-1} (the humidity was introduced by following through room-temperature water bubbler). The temperature increased to 700 °C firstly with a 2 °C/min ramping rate, and the sample was held to stabilize 1 h at this temperature, and subsequent temperature points down to 300 °C with 50 °C step size. The perturbation voltage of 10 mV and the frequency range of 0.01 Hz–5 MHz were used for the data collection. Obtained EIS results were analyzed by fitting with ZView software based on the equivalent circuit model to output resistances and then convert to conductivities.

3. Results

3.1. Crystal structures and microstructures

3.1.1. BZY20 green pellets

Fig. 1 summarizes the XRD patterns for the BZY20 green pellets after traditional dry pressing and cold sintering before the final sintering at 1500 °C. The XRD plot for the BZY20 precursor indicates the presence of minor $BaCO_3$ peak exists in the BZY20 precursor powder synthesized using the modified Pechini method with an eventual calcination temperature of 900 °C. For calcining the BZY20 powder, the calcination temperature lower than 950 °C or the inefficient air exchange in the box furnace usually resulted in a residual amount of $BaCO_3$ phase inside the BZY20 powder. In this work, the use of a low calcination temperature of 900 °C helped achieve BZY20 powder with a smaller particle for improving BZY20's sinterability. The BZY20 green pellets, after the pretreatment of traditional pressing and cold sintering without water (TS-0 and CS-0), maintained a cubic perovskite structure with a similar
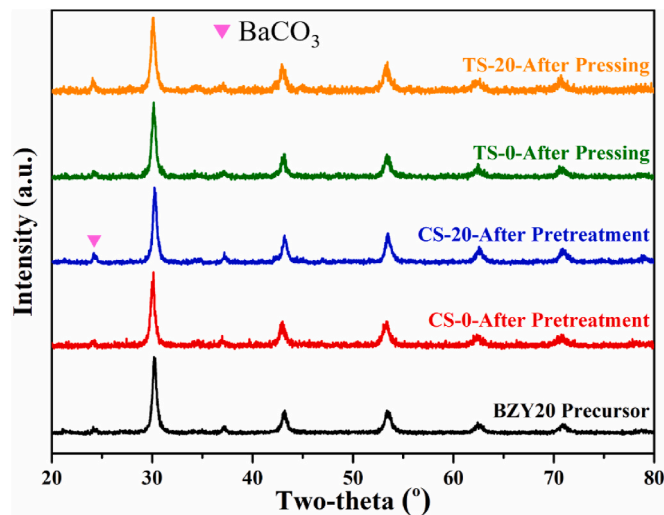
$BaCO_3$ peak intensity. However, the addition of 20 wt% of water for both traditional pressed and cold sintering pretreated BZY20 green pellets (TS-20 and CS-20) increased the peak intensity of $BaCO_3$. Pretreatment with 20 wt% H_2O addition resulted in the formation of a distinct $BaCO_3$ phase. The previous studies indicated that a proper amount of $BaCO_3$ in BZY20 could improve the BZY20's sinterability to achieve high relative density and large grains [14]. Therefore, we expect that the introduced $BaCO_3$ in BZY20 by the pretreatment with 20 wt% can increase the sintered BZY20 pellets' relative density.

The green histograms in Fig. 2 provide the relative densities of the BZY20 green pellets. The CS-20 BZY20 green pellet after cold sintering with 20 wt% water at 180 °C showed a relative density of ~76%, which was higher than the theoretical packing density of the cubic close-packing structure (~74%) based on equal spheres. The three other BZY20 green pellets of CS-0 (cold sintering without water), TS-0 (traditional pressing without water), and TS-20 (traditional pressing without 20 wt% water) showed relative densities much lower than the one for CS-20 green pellet (53–56% vs. 76%). Since the high relative density for the green pellets usually resulted in high relative density for the sintered pellets, we expect to achieve high relative density for the BZY20 pellets pretreated by cold sintering with 20 wt% at 180 °C.

Fig. 3 further provides the cross-section SEM images of the BZY20 green pellets cold sintered at 180 °C with and without water. The BZY20 green pellets cold sintered with 20% water (CS-20, Fig. 3b) showed a homogenous and highly compacted microstructure consistent with the high green relative density (Fig. 2, CS-20). The BZY20 green pellets cold sinter without water (CS-0, Fig. 3a) showed an inhomogenous and loosely packed microstructure consistent with the low green relative density (Fig. 2, CS-0). In summary, the CS-20 BZY20 green pellets cold sintered with 20 wt% water at 180 °C showed the proper amount of $BaCO_3$ as a sintering aid, high green relative density, and homogeneously compacted microstructure. Therefore, we expect to achieve improved sinterability for BZY20 green pellets cold sintered with 20 wt % water at 180 °C (CS-20 BZY20 green pellets).

3.1.2. BZY20 sintered pellets

Fig. 4 summarizes the XRD patterns for the BZY20 pellets sintered at 1500 °C for 12 h. The XRD patterns indicate that all the four sintered BZY20 pellets formed the pure cubic perovskite structure with a spacegroup of $Pm\overline{3}m$ with $BaCO_3$ impurity completely disappeared. The relative intensity, width, and position of the corresponding peaks for all four samples do not show a noticeable difference, which indicates crystal structures of the sintered BZY20 under different conditions was the same within our XRD analysis error range. In other words, different

Fig. 1. XRD patterns of BZY20 precursor powders and green pellets after cold sintering pretreatment and traditional pressing process with different water amounts. 22. (For interpretation of the references to colour in this figure legend, the reader is referred to the Web version of this article.)
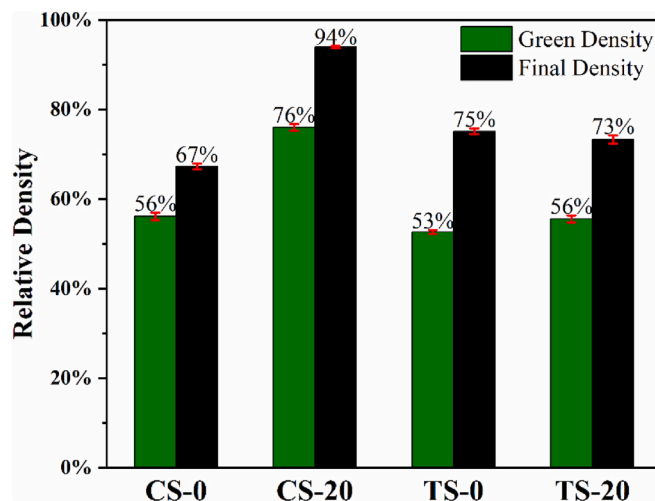
Fig. 2. The summary of relative densities (calculated by the geometric measurement) for all samples discussed. 23.
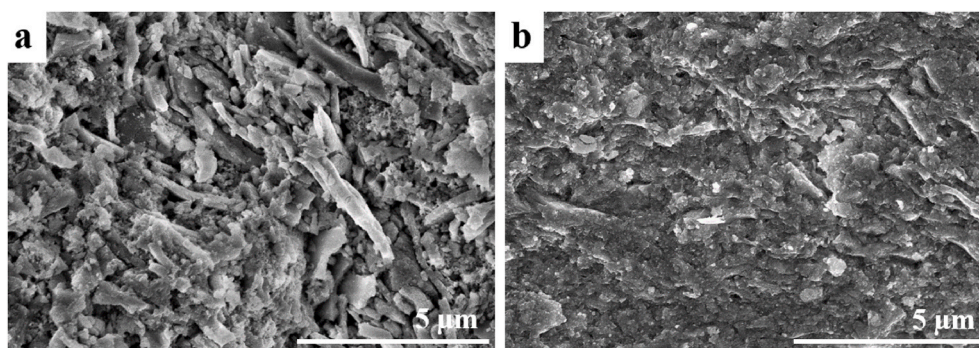
Fig. 3. The cross-sectional SEM images of CS-0 (a) and CS-20 (b) after cold sintering pretreatment. 23.
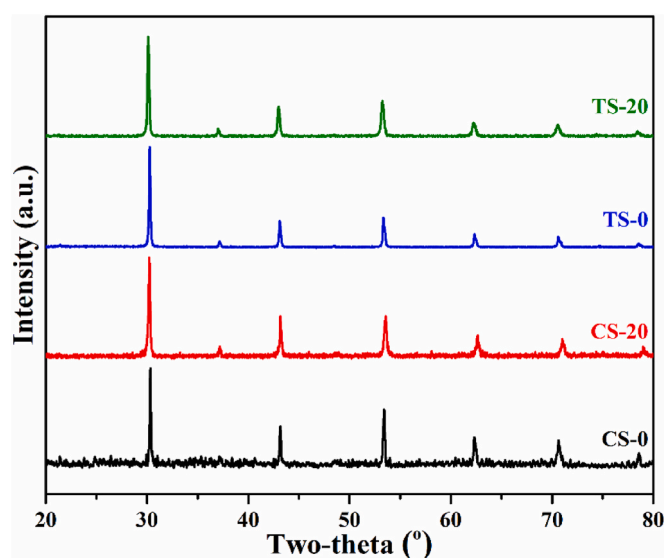
Fig. 4. XRD patterns of BZY20 pellets that fabricated with the cold sintering pretreatment and the traditional sintering method with different water amounts. 24.

pretreatment conditions (Table 1) for the BZY20 green pellets did not affect the eventual crystal structure of a fully sintered BZY20 pellet, which ensured good proton conduction properties.

The black histograms in Fig. 2 summarize the relative densities of the BZY20 pellets after the subsequent sintering at 1500 °C for 12 h. The CS-0, TS-0, and TS-20 BZY20 pellets after sintering resulted in much lower relative densities of 67%, 75%, and 73%, respectively. Considering the lower green relative densities and the less $BaCO_3$ sintering aid for CS-0 and TS-0 BZY20 green pellets, the poor sintering results for these three samples are reasonable. After a longer pressing process and higher temperature, even though the density of CS-0 was higher than TS-0, the inhomogeneous microstructure discussed above eventually leads to a much lower relative density after the final 1500 °C sintering (~67%) than TS-0. For TS-20, the addition of 20 wt% H_2O might somehow help to improve the packing density after 10 min pressing comparing with TS-0. Once the final 1500 °C sintering was conducted, the extra water just went without leaving any improvement as showing the similar relative density with TS-0 considering the experimental error (red bars in Fig. 2). In other words, the additional 20 wt% H_2O in the room temperature pressing does not affect the final relative density even though it may lead to a little bit of improvement for the density of green pellet. When cold sintering was applied, the added water could strongly interact with BZY20 powders rather than simple physical absorption. The CS-20 BZY20 pellets achieved a relative density as high as ~94% after the final sintering, consistent with its high green relative density,

homogeneous and compact microstructure, and a larger amount of $BaCO_3$ sintering aid.

Fig. 5 summarizes the fractured cross-sectional SEM images for all the four BZY20 pellets after sintering at 1500 °C for 12 h. The CS-20 BZY20 pellet does not show any obvious pores suggesting the high relative density. All the other three BZY20 pellets (CS-0, TS-0, and TS-20) show visible pores in the SEM micrographs in line with the low relative densities reported above. The further comparison of these four pellets' microstructures indicates that the sintered CS-20 pellets have grain sizes ~1 μm, almost twice those for the other three samples. Therefore, we can conclude that the cold sintering pretreatment with 20 wt% water at 180 °C for 1 h can efficiently assist the sintering process of the BZY20 pellets, which allowed the densification of the refractory BZY20. The densification temperature was lowered by about 200 °C compared to the traditional sintering method. The fully densified and large-grained microstructure should result in high proton conductivity.

3.2. Proton conductivity

Fig. 6 presents an examplar EIS spectrum measured at 300 °C under wet air condition for the symmetrical cell comprised of the sintered CS-20 BZY20 electrolyte and silver electrodes. The red square points show the Nyquist plot of EIS measurement results after area normalization. As is shown, the Nyquist plot consists of an intercept at the Z-Real axis at high frequency, two depressed small semicircles at intermediate-frequency range, and a straight line with ~45° relative to the Z-real axis at low-frequency range. The equivalent circuit model (inset in Fig. 6) was used to fit the EIS data points by Z-View software. For detail, the consisting of the elements of electrolyte bulk, electrolyte grain boundary, electrolyte-electrode interfacial charge transfer (protons), and electrode diffusion, The EIS Nyquist plots' analysis is the same as most protonic ceramic electrolyte symmetrical cells, allowing the achieving of electrolyte electrical conductivities quickly. The characteristic frequencies (f_{max}) and capacitance (C) are listed in Fig. 6, which fall in the similar value literature reported [26].

Fig. 7 displays the total conductivities of the CS-20 BZY20 under different atmospheres (dry air, wet air, dry 5% H_2, and wet 5% H_2) in the temperature range from 300 °C to 700 °C. It is consistent with most other reports that our BZY20 electrolyte pellets showed increased total electrical conductivities with increased temperature. The atmospheres showed a significant effect on the electrical conductivities at a specific fixed temperature. The total conductivities under wet atmospheres (wet air and wet 5% H_2) are much higher than those under dry atmospheres (dry air and dry H_2). The electrical transport activation energies showed the smallest value under dry 5% H_2 (i.e., 0.38 eV) and the largest value under dry air (i.e., 0.77 eV). While under wet atmospheres, the oxygen partial pressure did not affect the transport activation energies markedly. The activation energies under wet air and wet 5% H_2 are almost equal within the error range (0.51 eV vs. 0.48 eV). Besides, as the same as most proton conductivity under wet reducing atmosphere, the
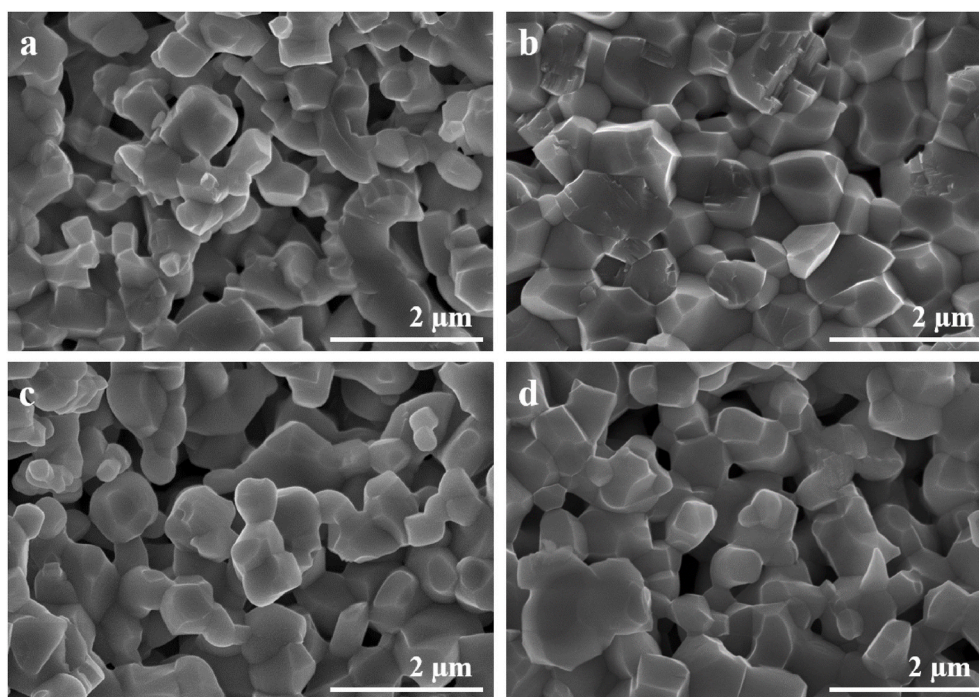
Fig. 5. The cross-sectional SEM images of CS-0 (a), CS-20 (b), TS-0 (c) and TS-20 (d). 25.
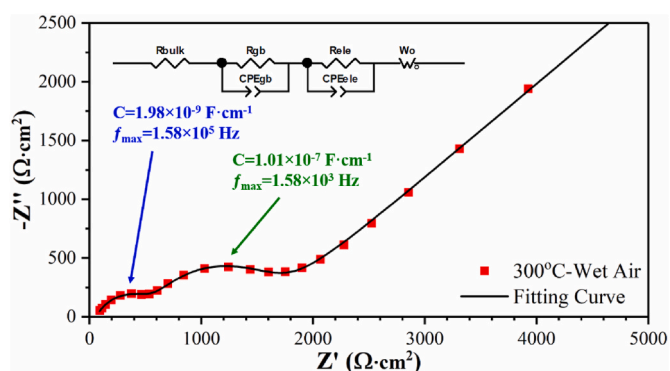
Fig. 6. The fitting of the EIS plot of the CS-20 sample was tested at 300 °C under wet air. Inset is the equivalent circuit used for fitting. 25.

activation energies showed relatively smaller values in the higher temperature range (500°C–700 °C) than at lower temperatures (300°C–500 °C). Furthermore, the CS-20 BZY20 pellets' total conductivities under wet atmospheres are among the representative BZY20 pellets' highest region [10,11,27–32].

4. Discussion

The study for the BZY20 pellets sintered at moderate temperature (i. e., 1500 °C) indicated that the pretreatment of green pellets by cold sintering at 180 °C with 20 wt% water could result in fully densified phase-pure BZY20 pellets. The cold sintering pretreatment could increase the barium carbonate amount inside the green pellet and the cold-sintered green pellet's relative density as described above. Therefore, we can ascribe the improved sinterability of the BZY20 pellets to these effects.

The total conductivities for the CS-20 BZY20 pellets under wet air and wet 5% H_2 both are much higher than the respective dry atmospheres (dry air and dry 5% H_2). The significantly higher electrical conductivities caused by water introduction come from the dominant
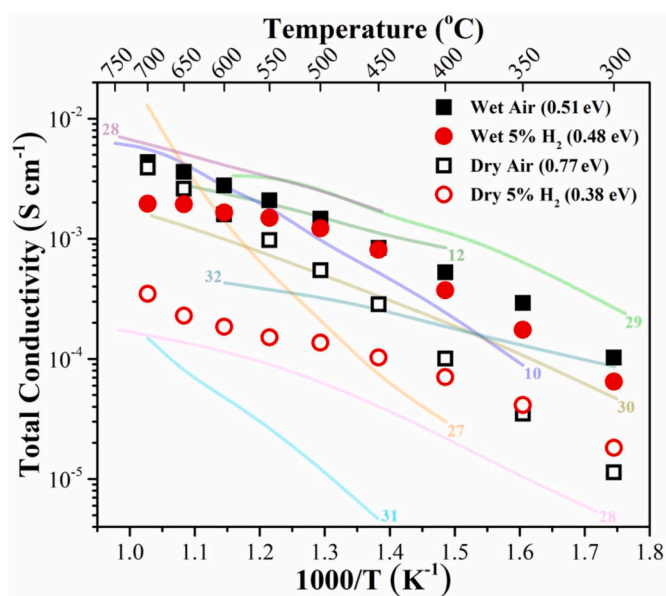
Fig. 7. The temperature dependence of total conductivity under different atmospheres for CS-20, with comparing with representative BZY20 under wet atmospheres. 26.

proton conductivity in wet atmospheres, which is the same as other proton conducting oxides. The electrical transport activation energies of ~0.5 eV are consistent with proton conduction in perovskite-type oxides (e.g., BZY20). The lower increasing rate (lower activation energy) at the high-temperature range (500–700 °C) for the BZY20 under wet 5% H_2 results from the decrease in proton concentration and a minor increase in proton mobility, which is consistent with most of the other proton conducting oxides too [33–35]. When the atmospheres turn into dry atmospheres (dry air and dry 5% H_2), the electrical conductivities are much lower than those achieved under wet atmospheres. The high electrical transport activation energy of 0.77 eV under dry air is

attributed to the lack of hydrogen or water in a dry air atmosphere. Thus, it is not surprised that the contribution of proton conductivity to the total conductivity is negligible. The lowest conductivity was observed with the test under dry 5% H_2. The lower concentration of protons in the BZY20 pellets due to the lack of water and the low oxygen partial pressure were hypothesized to result in a lower total conductivity. When we consider the activation energy, under dry 5% H_2 BZY20 shows the lowest value, even lower than the value observed under wet 5% H_2. The potential mixed ionic conduction (concomitant H^+ and O^{2-} transport) under a wet reducing atmosphere may cause the observed increased activation energy. Further studies aimed at understanding the conduction properties of the phase-pure and fully densified BZY20 are ongoing.

5. Conclusions

In summary, we demonstrate a cold sintering pretreatment of BZY20 helped to produce dense ceramics at a moderate temperature of 1500 °C (200 °C lower than the traditional sintering temperature). The as-fabricated BZY20 pellets showed a phase-pure perovskite structure, high relative density, and desired microstructure. A further comparative study with the control BZY20 pellets indicated introducing the proper amount of $BaCO_3$ on the precursor particle surface and the high green density for the green pellets with homogenous microstructure achieved by cold sintering pretreatment were responsible for lowering the final sintering temperature. Furthermore, the as-fabricated BZY20 pellets showed comparably high proton conductivity to conventionally processed state-of-the-art BZY20 pellets. We expect to utilize this fabrication method for other protonic ceramic electrolyte membranes.

Declaration of competing interest

The authors declare that they have no known competing financial interests or personal relationships that could have appeared to influence the work reported in this paper.

References

[1] Z. Zhao, J. Cui, M. Zou, S. Mu, H. Huang, Y. Meng, K. He, K.S. Brinkman, J. (Joshua, Tong, Novel twin-perovskite nanocomposite of Ba–Ce–Fe–Co–O as a promising triple conducting cathode material for protonic ceramic fuel cells, J. Power Sources 450 (2020) 227609, https://doi.org/10.1016/j.jpowsour.2019.227609.

[2] C. Duan, J. Tong, M. Shang, S. Nikodemski, M. Sanders, S. Ricote, A. Almansoori, R. O'Hayre, Readily processed protonic ceramic fuel cells with high performance at low temperatures, Science 349 (2015) 1321–1326, https://doi.org/10.1126/science.aab3987.

[3] L. Bi, S. Boulfrad, E. Traversa, Steam electrolysis by solid oxide electrolysis cells (SOECs) with proton-conducting oxides, Chem. Soc. Rev. 43 (2014) 8255–8270, https://doi.org/10.1039/c4cs00194j.

[4] M. Marrony, J. Dailly, Advanced proton conducting ceramic cell as energy storage device, J. Electrochem. Soc. 164 (2017) F988–F994, https://doi.org/10.1149/2.1541709jes.

[5] H. Iwahara, Y. Asakura, K. Katahira, M. Tanaka, Prospect of hydrogen technology using proton-conducting ceramics, Solid State Ionics 168 (2004) 299–310, https://doi.org/10.1016/j.ssi.2003.03.001.

[6] K.D. Kreuer, Proton-conducting oxides, Annu. Rev. Mater. Res. 33 (2003) 333–359, https://doi.org/10.1146/annurev.matsci.33.022802.091825.

[7] H. Iwahara, T. Yajima, H. Ushida, Effect of ionic radii of dopants on mixed ionic conduction (H^++O^{2-}) in $BaCeO_3$-based electrolytes, Solid State Ionics 70 (1994) 267–271, https://doi.org/10.1016/0167-2738(94)90321-2.

[8] Z. Zhong, Stability and conductivity study of the $BaCe_{0.9-x}Zr_xY_{0.1}O_{2.95}$ systems, Solid State Ionics 178 (2007) 213–220, https://doi.org/10.1016/j.ssi.2006.12.007.

[9] A. VahidMohammadi, Z. Cheng, Fundamentals of synthesis, sintering issues, and chemical stability of $BaZr_{0.1}Ce_{0.7}Y_{0.1}Yb_{0.1}O_{3-\delta}$ proton conducting electrolyte for

[10] E. Fabbri, A. D'Epifanio, E. Di Bartolomeo, S. Licoccia, E. Traversa, Tailoring the chemical stability of $Ba(Ce_{0.8-x}Zr_x)Y_{0.2}O_{3-\delta}$ protonic conductors for intermediate temperature solid oxide fuel cells (IT-SOFCs), Solid State Ionics 179 (2008) 558–564, https://doi.org/10.1016/j.ssi.2008.04.002.

[11] L. Bi, E. Traversa, Synthesis strategies for improving the performance of doped-$BaZrO_3$ materials in solid oxide fuel cell applications, J. Mater. Res. 29 (2014) 1–15, https://doi.org/10.1557/jmr.2013.205.

[12] C. Peng, J. Melnik, J.L. Luo, A.R. Sanger, K.T. Chuang, $BaZr_{0.8}Y_{0.2}O_{3-\delta}$ electrolyte with and without ZnO sintering aid: preparation and characterization, Solid State Ionics 181 (2010) 1372–1377, https://doi.org/10.1016/j.ssi.2010.07.026.

[13] Y. Yamazaki, R. Hernandez-Sanchez, S.M. Haile, Cation non-stoichiometry in yttrium-doped barium zirconate: phase behavior, microstructure, and proton conductivity, J. Mater. Chem. 20 (2010) 8158–8166, https://doi.org/10.1039/c0jm02013c.

[14] Y. Yamazaki, R. Hernandez-Sanchez, S.M. Haile, High total proton conductivity in large-grained yttrium-doped barium zirconate, Chem. Mater. 21 (2009) 2755–2762, https://doi.org/10.1021/cm900208w.

[15] S. Wang, Y. Liu, J. He, F. Chen, K.S. Brinkman, Spark-plasma-sintered barium zirconate based proton conductors for solid oxide fuel cell and hydrogen separation applications, Int. J. Hydrogen Energy 40 (2015) 5707–5714, https://doi.org/10.1016/j.ijhydene.2015.02.116.

[16] S. Ricote, N. Bonanos, H.J. Wang, B.A. Boukamp, Conductivity study of dense $BaZr_{0.9}Y_{0.1}O_{3-\delta}$ obtained by spark plasma sintering, Solid State Ionics 213 (2012) 36–41, https://doi.org/10.1016/j.ssi.2011.02.011.

[17] N. Sata, Y. Shibata, F. Iguchi, H. Yugami, Crystallization process of perovskite type oxide thin films deposited by PLD without substrate heating: influence of sputtering rate and densification-driven high tensile strain, Solid State Ionics 275 (2015) 14–18, https://doi.org/10.1016/j.ssi.2015.02.005.

[18] J. Tong, D. Clark, M. Hoban, R. O'Hayre, Cost-effective solid-state reactive sintering method for high conductivity proton conducting yttrium-doped barium zirconium ceramics, Solid State Ionics 181 (2010) 496–503, https://doi.org/10.1016/j.ssi.2010.02.008.

[19] D. Han, Y. Otani, K. Goto, S. Uemura, M. Majima, T. Uda, Electrochemical and structural influence on $BaZr_{0.8}Y_{0.2}O_{3-\delta}$ from manganese, cobalt, and iron oxide additives, J. Am. Ceram. Soc. 103 (2020) 346–355, https://doi.org/10.1111/jace.16748.

[20] D. Gao, R. Guo, Structural and electrochemical properties of yttrium-doped barium zirconate by addition of CuO, J. Alloys Compd. 493 (2010) 288–293, https://doi.org/10.1016/j.jallcom.2009.12.082.

[21] J. Li, C. Wang, X. Wang, L. Bi, Sintering aids for proton-conducting oxides – a double-edged sword? A mini review, Electrochem. Commun. 112 (2020) 106672, https://doi.org/10.1016/j.elecom.2020.106672.

[22] H. Guo, A. Baker, J. Guo, C.A. Randall, Protocol for ultralow-temperature ceramic sintering: an integration of nanotechnology and the cold sintering process, ACS Nano 10 (2016) 10606–10614, https://doi.org/10.1021/acsnano.6b03800.

[23] J. Guo, H. Guo, A.L. Baker, M.T. Lanagan, E.R. Kupp, G.L. Messing, C.A. Randall, Cold sintering: a paradigm shift for processing and integration of ceramics, Angew. Chem. Int. Ed. 55 (2016) 11457–11461, https://doi.org/10.1002/anie.201605443.

[24] H. Guo, J. Guo, A. Baker, C.A. Randall, Hydrothermal-assisted cold sintering process: a new guidance for low-temperature ceramic sintering, ACS Appl. Mater. Interfaces 8 (2016) 20909–20915, https://doi.org/10.1021/acsami.6b07481.

[25] K. Thabet, E. Quarez, O. Joubert, A. Le Gal La Salle, Application of the cold sintering process to the electrolyte material $BaCe_{0.8}Zr_{0.1}Y_{0.1}O_{3-\delta}$, J. Eur. Ceram. Soc. 40 (2020) 3445–3452, https://doi.org/10.1016/j.jeurceramsoc.2020.03.043.

[26] J.G. Lyagaeva, G.K. Vdovin, D.A. Medvedev, Distinguishing bulk and grain boundary transport of a proton-conducting electrolyte by combining equivalent circuit scheme and distribution of relaxation times analyses, J. Phys. Chem. C 123 (2019) 21993–21997, https://doi.org/10.1021/acs.jpcc.9b05705.

[27] J. Gao, Y. Liu, Y. Meng, M. Hu, K.S. Brinkman, Fluoride-based anion doping: a new strategy for improving the performance of protonic ceramic conductors of the form $BaZrO_3$, ChemElectroChem 7 (2020) 2242–2247, https://doi.org/10.1002/celc.202000154.

[28] S. Tao, J.T.S. Irvine, Conductivity studies of dense yttrium-doped $BaZrO_3$ sintered at 1325 °C, J. Solid State Chem. 180 (2007) 3493–3503, https://doi.org/10.1016/j.jssc.2007.09.027.

[29] K. Nomura, H. Kageyama, Transport properties of $Ba(Zr_{0.8}Y_{0.2})O_{3-\delta}$ perovskite, Solid State Ionics 178 (2007) 661–665, https://doi.org/10.1016/j.ssi.2007.02.010.

[30] R.B. Cervera, Y. Oyama, S. Miyoshi, K. Kobayashi, T. Yagi, S. Yamaguchi, Structural study and proton transport of bulk nanograined Y-doped $BaZrO_3$ oxide protonics materials, Solid State Ionics 179 (2008) 236–242, https://doi.org/10.1016/j.ssi.2008.01.082.

[31] Z. Sun, E. Fabbri, L. Bi, E. Traversa, Electrochemical properties and intermediate-temperature fuel cell performance of dense yttrium-doped barium zirconate with calcium addition, J. Am. Ceram. Soc. 95 (2012) 627–635, https://doi.org/10.1111/j.1551-2916.2011.04795.x.

[32] W. Sun, Z. Shi, M. Liu, L. Bi, W. Liu, An easily sintered, chemically stable, barium zirconate-based proton conductor for high-performance proton-conducting solid oxide fuel cells, Adv. Funct. Mater. 24 (2014) 5695–5702, https://doi.org/10.1002/adfm.201401478.

[33] K.Y. Park, Y. Seo, K.B. Kim, S.J. Song, B. Park, J.Y. Park, Enhanced proton conductivity of yttrium-doped barium zirconate with sinterability in protonic

ceramic fuel cells, J. Alloys Compd. 639 (2015) 435–444, https://doi.org/10.1016/j.jallcom.2015.03.168.

[34] K. Yang, J.X. Wang, Y.J. Xue, M. Sen Wang, C.R. He, Q. Wang, H. Miao, W. G. Wang, Synthesis, sintering behavior and electrical properties of Ba $(Zr_{0.1}Ce_{0.7}Y_{0.2})O_{3-\delta}$ and $Ba(Zr_{0.1}Ce_{0.7}Y_{0.1}Yb_{0.1})O_{3-\delta}$ proton conductors, Ceram. Int. 40 (2014) 15073–15081, https://doi.org/10.1016/j.ceramint.2014.06.115.

[35] A. Lesnichyova, A. Stroeva, S. Belyakov, A. Farlenkov, N. Shevyrev, M. Plekhanov, I. Khromushin, T. Aksenova, M. Ananyev, A. Kuzmin, Water uptake and transport properties of $La_{1-x}Ca_xScO_{3-\alpha}$ proton-conducting oxides, Materials 12 (2019) 2219, https://doi.org/10.3390/ma12142219.